

Energy-sensitive imaging detector applied to the dissociative recombination of D_2H^+

H. Buhr,^{1,2,*} M. B. Mendes,² O. Novotný,² D. Schwalm,^{1,2} M. H. Berg,² D. Bing,² O. Heber,¹
C. Krantz,² D. A. Orlov,² M. L. Rappaport,¹ T. Sorg,² J. Stützel,² J. Varju,² A. Wolf,² and D. Zajfman¹

¹*Faculty of Physics, Weizmann Institute of Science, 76100 Rehovot, Israel*

²*Max-Planck-Institut für Kernphysik, 69121 Heidelberg, Germany*

(Dated: November 21, 2018)

We report on an energy-sensitive imaging detector for studying the fragmentation of polyatomic molecules in the dissociative recombination of fast molecular ions with electrons. The system is based on a large area ($10 \times 10 \text{ cm}^2$) position-sensitive, double-sided Si-strip detector with 128 horizontal and 128 vertical strips, whose pulse height information is read out individually. The setup allows to uniquely identify fragment masses and is thus capable of measuring branching ratios between different fragmentation channels, kinetic energy releases, as well as breakup geometries, as a function of the relative ion-electron energy. The properties of the detection system, which has been installed at the TSR storage ring facility of the Max-Planck Institute for Nuclear Physics in Heidelberg, is illustrated by an investigation of the dissociative recombination of the deuterated triatomic hydrogen cation D_2H^+ . A huge isotope effect is observed when comparing the relative branching ratio between the D_2+H and the $HD+D$ channel; the ratio $2B(D_2+H)/B(HD+D)$, which is measured to be 1.27 ± 0.05 at relative electron-ion energies around 0 eV, is found to increase to 3.7 ± 0.5 at ~ 5 eV.

PACS numbers: 34.80.Lx, 34.80.Ht, 34.80.Gs

I. INTRODUCTION

Dissociative recombination (DR) with electrons is the most important loss channel for molecular ions in cold dilute plasmas and a source of energetic neutral atoms and excited molecules [1]. Rate coefficients, branching ratios, and the energy sharing between internal and external degrees of freedom of the fragments are thus important ingredients in modeling these plasmas. Even though a good understanding of the DR process of diatomic molecular ions has been reached in recent years, theory is not yet capable of supplying most of the information needed for these studies. Experimental investigations of the DR process in particular of polyatomic systems are thus still indispensable to further constrain the parameters of these models and to provide basic theory with detailed and reliable results for crucial benchmark systems.

Considerable experimental progress in studying the DR process has been made since the advent of heavy-ion storage rings with merging electron beam facilities, which allow to control the inner excitation of the molecular ions and the relative ion-electron energy precisely enough to produce data in the parameter space of interest for, e.g., planetary atmospheres or interstellar chemistry. Results obtained so far were vital in helping to unravel the processes governing the DR and to clarify many important and pertinent issues. But despite these experimental advances for particular diatomic systems, detailed investigations of the DR of more complex ions, such as measurements of branching ratios at relative energies other than zero, of the inner excitation of the molecular fragments or of their dissociation kinematics, are still hampered due to

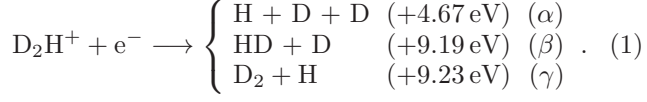
the limitations of presently available detection techniques in identifying the DR reaction products.

We have therefore developed an **E**nergy-sensitive **M**ulti-strip detector system (EMU) that is capable of recording multi-fragment events following the DR of polyatomic molecular ions and to identify the fragments by their masses. The system has been installed at the ion storage ring TSR of the Max-Planck Institute for Nuclear Physics, which can store molecular ions of MeV energies and is equipped with an electron cooler as well as an electron target employing a cryogenic photocathode, so that electron-ion collision energies can be freely set in the meV to eV range with unprecedented resolution [2]. While the main aim of the setup is to provide a universal tool for measuring DR branching ratios of polyatomic molecular ions into the different final fragment channels, the position resolution is sufficient to allow also for 2D imaging of the breakup geometries. The new setup has thus several advantages as compared to previous approaches [3], where grids of different transmissions (yielding a set of linear combinations of the rates for individual fragment channels) were employed in order to determine the branching ratios, a technique which is usually only applied at zero relative electron-ion energies for background reasons and which does not support molecular imaging.

The present paper discusses the concept and realization of the EMU detection system and exemplifies its properties and possibilities by using the new setup to investigate the dissociative recombination of D_2H^+ . The DR of D_2H^+ was studied before in several storage ring experiments, and rate coefficients [4, 5], the fragmentation geometry of the three-body channel [6], and branching ratios [5] have been reported. The kinetic energy Q_0 released in the three fragmentation channels, for ions and fragments in their ground states and relative ion-electron

*Corresponding author: henrik.buhr@mpi-hd.mpg.de

energies $E_e = 0$ eV, are



The branching ratios measured at $E_e \sim 0$ eV were reported to be $B_\alpha=76.5(2.2)\%$, $B_\beta=13.5(1.5)\%$, and $B_\gamma=10.0(0.7)\%$ [5].

II. THE DETECTOR CONCEPT

Since the beam energies E_B of the molecular ions stored in the TSR are very large as compared to the release energies occurring in DR experiments, the fragments resulting from a DR event of a molecular ion of mass number A are traveling within a narrow cone around the ion beam axis, and the kinetic energy E_i of the fragment i is to a very good approximation given by

$$E_i = \frac{A_i}{A} E_B \quad (2)$$

and is thus a measure of the mass number A_i of the fragment. By recording separately the energies of all DR fragments of an DR event with a large area multi-hit-capable detector the fragmentation channel can be uniquely identified.

In the present setup the energy-sensitive multi-hit detector is realized by a large area ($10 \times 10 \text{ cm}^2$) position-sensitive, double-sided Si-strip detector (see Fig. 1). The energy- and position-sensitivity to particles hitting the detector is achieved through 128 vertical (x-) and 128 horizontal (y-) strips on the front and back side of the detector, respectively, which are read out individually by preserving the pulse height, i.e., the energy information. The readout system also ensures via the timing information that the detected particles belong to a single DR event. The detector is mounted about $S \approx 10 \text{ m}$ downstream of the electron target outside of the magnetic lattice of the TSR such that it can only be hit by neutral fragments.

The impact of n fragments from a single DR event on the detector leads to n_x responding x-strips x_i and n_y responding y-strips y_i with corresponding energies E_{x_i} and E_{y_i} , and the detection of all fragments can be easily verified by checking whether the two energy relations

$$\sum_{i=1}^{n_x} E_{x_i} = E_B \text{ and } \sum_{i=1}^{n_y} E_{y_i} = E_B \quad (3)$$

are fulfilled. The measured fragment mass numbers A_{x_i} and A_{y_i} corresponding to the energies recorded on the individual strips are given by

$$A_{x_i} = A E_{x_i} / E_B \text{ and } A_{y_i} = A E_{y_i} / E_B. \quad (4)$$

In the following we will refer to the set of measured mass numbers A_{x_i} , A_{y_i} and the corresponding strip coordinates x_i , y_i as the 'hit pattern' of the DR event.

The coordinates of the center-of-mass (x_{cm}, y_{cm}) of the detected event in the detector plane are given by

$$(x_{cm}, y_{cm}) = 1/A \left(\sum_{i=1}^{n_x} A_{x_i} x_i, \sum_{i=1}^{n_y} A_{y_i} y_i \right), \quad (5)$$

and an estimate for the transversal kinetic energy release E_\perp can be determined from the projected weighted distances D^2 defined by

$$D^2 = \sum_{i=1}^{n_x} \frac{A_{x_i}}{A} (x_i - x_{cm})^2 + \sum_{i=1}^{n_y} \frac{A_{y_i}}{A} (y_i - y_{cm})^2 \quad (6)$$

using

$$E_\perp = E_B \times D^2 / S^2, \quad (7)$$

where S is the distance between the center of the electron target and the detector.

While Eqs. (3)-(7) are valid even in cases where more than one fragment hit the same strip, the strip-wise readout of only two coordinate planes together with the finite strip width leads to ambiguities in the determination of the breakup geometry from the hit pattern, which in some cases also affects the identification of the fragmentation channel. We shall first discuss these ambiguities for the specific case of the DR of D_2H^+ , before we consider the more general case.

Figure 2 depicts the two most frequent of these ambiguities. The hit pattern shown in Fig. 2(a) is indistinguishable from the hit pattern shown in Fig. 2(b); this pattern thus results in two solutions concerning the fragmentation geometry. However, the identification of the fragmentation channel is still unique. This is no longer the case for the hit pattern shown in Fig. 2(c), where the H and the two Ds from the 3-body fragmentation channel are forming an L-shaped pattern with the H in the corner such that only two horizontal and two vertical strips are responding. This pattern cannot be distinguished from

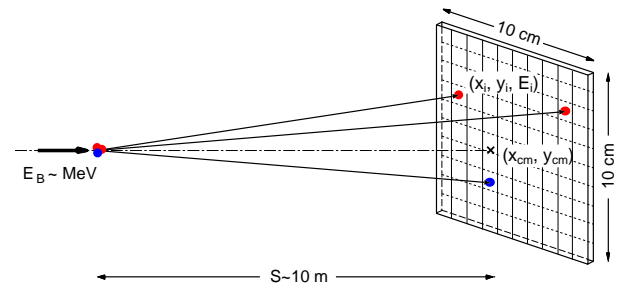


FIG. 1: Concept of the EMU detector: A fast, neutralized molecule is dissociating at a distance S from a position- and energy-sensitive detector. The fragments continue to travel approximately at the velocity of the molecule, but due to the kinetic energy released in the dissociation they acquire macroscopic distances from the transversal center-of-mass (x_{cm}, y_{cm}) when hitting the detector. The position (x_i, y_i) and the energy E_i of each fragment is recorded.

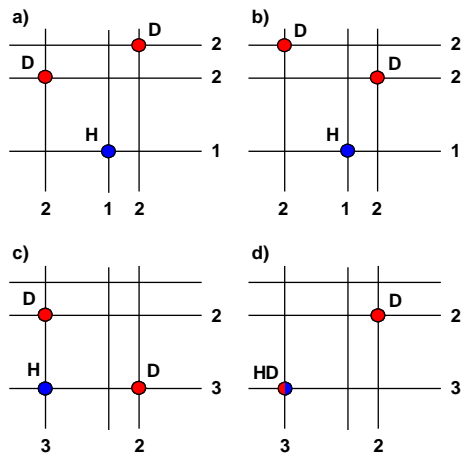


FIG. 2: Some breakup geometries and corresponding hit pattern occurring in the DR of D_2H^+ . The lines mark the responding read-out strips in vertical (x_i) and horizontal (y_i) directions; the numbers at the end are the mass numbers A_{x_i} and A_{y_i} derived with Eq. (4). The breakup geometries shown in a) and c) result in the same read-out pattern (hit pattern) as the geometries shown in b) and d), respectively. But while the hit pattern resulting from the geometries shown in a) and b) still allow unique identification of the fragmentation channel, the pattern resulting from the breakup geometries depicted in c) and d) is ambiguous with respect to the fragmentation channels D+D+H and HD+D.

that shown in Fig. 2(d), which results from the detection of a molecular HD- and an atomic D-fragment from the 2-body channel (β). Besides the even less likely occurrence of two or more fragments hitting the same x- and y-strip, i.e., the same (x, y) -pixel, these L-shaped patterns are the only patterns in the DR of D_2H^+ , which cannot be attributed uniquely to a fragmentation channel. Since the probability for the occurrence of this pattern is small due to the narrow strip width of $730 \mu m$ realized in the present setup, we attribute these patterns to the channel with the smaller number of fragments, that is for the case discussed in Figs. 2(c,d) to the HD+D channel. The influence of these miss-assignments on the accuracy of the branching ratios is small and can moreover be corrected for with the help of Monte Carlo simulations (see also Sec. V A).

While the ambiguities caused by fragments hitting the same (x, y) pixel discussed above are present in case of all molecules, the other ambiguities depend on the multiplicity of identical fragment masses in the open fragmentation channels. In the DR of polyatomic molecules consisting of atoms of different masses such as HCO^+ , the identification of the fragmentation channel and of the fragmentation geometry is not subject to any other ambiguities. In the DR of polyatomic molecules, which contain several atoms of the same mass and fragment into channels containing two or more identical fragments, the main ambiguities hampering the identification of the fragmentation channels are again due to the L-shaped

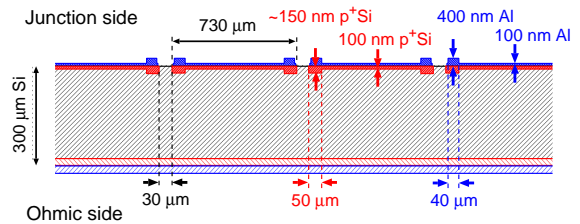


FIG. 3: Schematic cross section through the EMU detector, a double-sided, fully depleted Si-strip detector of $10 \times 10 cm^2$ active surface area. The p^+Si and the Al layers of the junction contact, through which the particles enter the detector, were made as thin as possible to minimize the energy losses of the DR fragments in these dead layers.

(sub-)pattern involving two identical fragments at the two ends of the L. The interpretation of hit patterns in terms of the fragmentation geometries is subject to similar ambiguities as discussed above, but the number of geometries leading to a specific pattern will strongly increase with the number of identical fragments. However, we again would like to point out that the center-of-mass determination by Eq. (5) and the transverse energy distribution defined by Eq. (7) are independent of these ambiguities.

III. EXPERIMENTAL SETUP

A. The EMU detection system

The large area double-sided Si strip detector employed in the EMU detection system was built by the UK physics company Micron Semiconductor Limited [7]. The detector has an active area of $97.3 mm \times 97.3 mm$ and an active depth of $300 \mu m$ when biased by $\leq -70 V$ (Fig. 3). Position sensitivity has been achieved by electronically subdividing the junction side into 128 vertical strips of $730 \mu m$ width, which are separated by gaps of $30 \mu m$, and the ohmic side in 128 horizontal strips of $700 \mu m$ width, which are separated by gaps of $60 \mu m$.

The thickness of the entrance (junction) window, which consists of a $100 nm$ -thick p^+ doped Si layer covered with a $100 nm$ -thick aluminum coating, was minimized in order to keep the energy loss in the inert window material, and thus the cut-off energy for the detection of the heavy DR fragments, as small as possible. The increased thicknesses of the p^+Si and the Al layer at the edges of the strips, which ensure a clean separation between the strips and a loss-free readout and which affect about 14 % of the active area of the detector, result in additional, slightly down-shifted peaks in the pulse height spectra; particles traversing this part of the entrance window suffer a larger energy loss which is specific for the fragment energy, mass, and its nuclear charge. This is discussed in more detail in Sec. IV in connection with the pulse height spectrum (Fig. 6) observed in the DR of

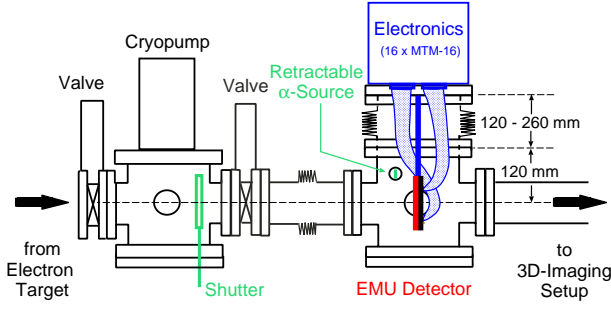


FIG. 4: Schematic view of the EMU setup, which is located in the BAMBI beamline downstream of the electron target of the TSR.

D_2H^+ . Since the penetration depth of the fragments in the detector material for energies available at the TSR is in most cases less than $10 \mu m$ and the gap region close to the surface is almost field-free, fragments impinging in the gap region, covering about 4 % of the detector surface, will likely not be detected.

The detector is mounted in a dedicated chamber (Fig. 4) in the neutral fragment beamline BAMBI downstream of the electron target [2] of the TSR. The distance from the center of the electron target to the front face of the detector is $S_0 = 941(1)$ cm. At this distance the detector covers the full cone size for the DR fragments that is allowed by the beamtube (CF100). The maximum visible cone is in fact limited vertically by the height of the vacuum chamber in the TSR dipole magnet to about 8 cm diameter. A large bellow allows to retract the detector out of the beamline so that experiments with detectors further down the beamline are possible without breaking the vacuum. Moreover, the detector can be moved up and down in front of a retractable α -source, which in turn can be moved horizontally using a translational stage, so that any part of the detector can be irradiated for testing and calibration purposes. The cryopump is vibrationally decoupled from the detector chamber to protect the wire bonds to the 256 strips of the detector from the mechanical noise of the pump. Under running conditions the vacuum in the detection chamber is about 5×10^{-9} mbar. A mechanical shutter is furthermore installed in the pumping chamber to protect the detector during the injection phase of the ion beam into the storage ring.

The 256 strips of the detector are read out by 16 highly integrated MTM-16 units developed by Mesytec [8], which are mounted directly on the upper lid of the detector chamber to minimize the length of the cables between detector and preamplifier. Each unit contains 16 channels consisting of a preamplifier, main amplifier, shaper and hold stage. Moreover, four input signals are added and compared to an adjustable discriminator level. The eight boards connected to the 128 x-strips and the eight boards serving the y-strips are daisy-chained to the two function blocks, respectively, of an MDI-2 unit developed by Mesytec as well. This one-slot VME unit allows one

to do all the controlling, timing and read out of the 16 MTM-16 boards. A trigger signal is produced when one of the discriminators of the 16 MTM-16 units responded; it activates the hold stages of the MTM-16 units after $2 \mu s$, (i.e., only signals arriving within this time will be held) and starts the readout sequence. The individual pulse heights are digitized by a sliding scale ADC and - if above a programmable threshold - stored together with the strip number in a FIFO, which is read out via the VME interface. In the present configuration the read-out speed is limited to about 2000 events per second. A schematic view of the electronic set up is shown in Fig. 5.

B. Specific settings for measuring the DR of D_2H^+

The first application of the EMU detection system was the investigation of the dissociative recombination of D_2H^+ . D_2H^+ ions were produced in a Penning source, accelerated to $E_B = 2.39$ MeV using an rf-quadrupole accelerator, and injected into the TSR; the stored ion current was up to about $4 \mu A$. After injection the ion beam was first phase-space cooled by the velocity-matched electron beam supplied by the electron target, which had a density of $9 \times 10^6 \text{ cm}^{-3}$ and a transversal temperature of approximately 1.5 meV (expansion factor 20). At these conditions the effective length of the electron target is 115 cm, with an additional 20 cm on either end where the electron beam is merged with and demerged from the ion beam. After a few seconds the ion beam was phase-space cooled to a beam diameter below 1.0 mm.

The electron beam was then used as a target, either at matched or detuned electron velocities. The detuning energy E_d , which measures the average electron-ion collision energy in the center-of-mass system, was adjusted to values between 0 and 20 eV by changing the acceleration voltage of the electron beam. At detuning energies $E_d > 0$ the electron beam velocity was switched at a rate of 10 - 100 Hz between $E_d = 0$ and the required energy E_d in order to keep the ion beam phase-spaced cooled. Data was recorded between a few seconds and up to 30 s after injection, and count rates were limited to ≤ 2 kHz.

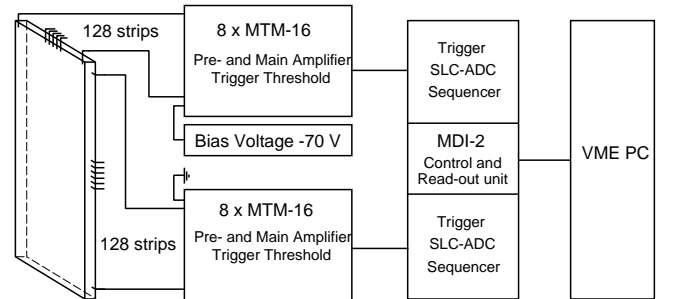


FIG. 5: A schematic view of the electronic setup for the EMU detector.

IV. DATA ANALYSIS

The first analysis step consists of shifting the pulse height spectra of the individual strips to a common scale in order to compensate for the slightly different amplifications and offsets of the individual electronic channels using the D_2H^+ data.

The sums of all 128 x- and of all 128 y-strip spectra performed after this calibration step, are displayed in Fig. 6. While the overall energy resolution reached with the y-strips on the back side of the detector (e.g., $\Delta E(\text{FWHM}) < 30$ keV for Ds of 0.96 MeV) is already very satisfactory, the resolution of the front side strips is worse by almost a factor of two. This is mainly due to the excess noise observed on the front side strips; while the back side of the detector is electronically well-shielded by a metal plate mounted directly behind the detector, the front side is unshielded in the direction of the storage ring. But although the resolution of the x-strips is not yet perfect, the peaks corresponding to the detection of an H, D, HD (or H+D), and D_2 (or D+D) can be clearly identified. Even the small peak is visible that is caused by the detection of all fragments (D_2H) on a single strip.

On the low-energy side of the peaks small satellite lines are visible. As already pointed out in Sec. III A these satellites are caused by particles passing through the slightly thicker parts of the entrance window. For light fragments as in the present case of the DR of D_2H^+ the resulting energy difference between the main and the satellite peak is small and thus does not hamper the mass assignment. For heavier fragments like carbon or oxygen, the energy difference will be larger and can correspond to one or more mass units. But even in these cases this will not lead to a misinterpretation of a DR event as the two energy sums [see Eq. (3)] will not be fulfilled. Disregarding these events, however, reduces the detection efficiency of the set-up and has to be taken into account by detailed simulations.

A more careful examination of Fig. 6(b) reveals a small number of counts between the peaks. These are mainly caused by events where the charges created by a fragment in the active volume of the detector are drifting to two adjacent y-strips such that the charge collected by each strip results in a reduced signal height. Such a pulse height splitting can be at least partly reconstructed by adding the signals of the two adjacent y-strips. A corresponding pulse height splitting on the front side of the detector is very unlikely to occur [see also Fig. 6(a)] as the range of the fragments in the detector material is so small that fragments hitting the gap between the x-strips are likely not be detected at all. As in the case discussed above, the influence of these effects on the detection efficiency is taken into account by simulations.

After the calibration procedure the pulse height of each of the 256 strips is compared to appropriately chosen windows around the mass peaks and, if it falls into one of these windows, the corresponding mass number is as-

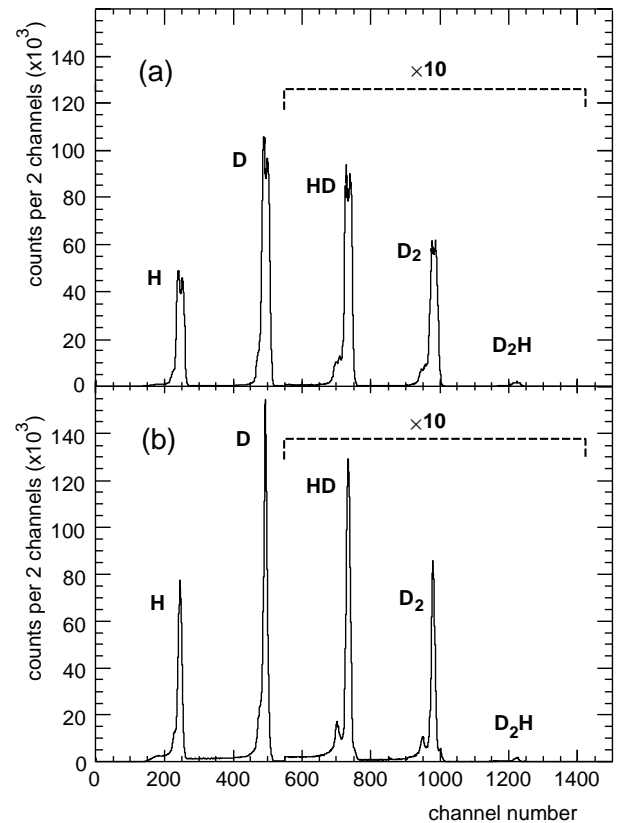


FIG. 6: Pulse height spectra obtained in the DR of 2.39 MeV D_2H^+ ions at a detuning energy of $E_d = 0$ eV. The figure shows the sum of the calibrated pulse height spectra (a) of all x-strips on the front and (b) of all y-strips on the back side. Above channel 550, counts are multiplied by a factor of 10.

signed to the strip. If the pulse height is above the lower threshold but does not fall into one of the mass windows, it is tested whether the sum with one of the neighboring strips fulfills this criterion. If yes, the corresponding mass is assigned to the strip with the larger signal while the other strip is ignored in the further analysis. We shall refer to this set of A_{x_i} and A_{y_j} and adjusted positions x_i and y_j , which are randomized across the width of the respective strip to avoid binning problems, as a hit pattern.

The next analysis step consists of checking whether the sums over all mass numbers A_{x_i} and A_{y_j} , respectively, observed in an event are equal to the mass number of the dissociating molecule, and whether the hit pattern corresponds to a possible DR fragmentation channel, i.e., whether there is any combination of the atomic constituents of the dissociating molecule that can explain the observed hit pattern. If yes, the event is marked as a DR event and the final fragment channel is assigned. Here, preference is given to the fragmentation channel with the smallest number of fragments. In the case of the DR of D_2H^+ , for example, this means that the rather unlikely L-shaped hit pattern shown in Fig. 2(c), which results from the three-body breakup and cannot be distinguished

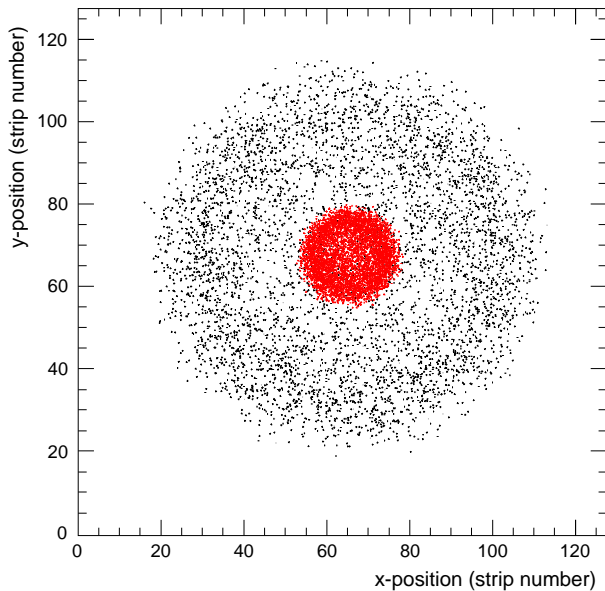


FIG. 7: The distribution of the H (black) and D_2 (red) positions observed for 5000 D_2+H events following the DR of D_2H^+ at $E_d=0$ eV. Note that H events within the red area are partly shadowed by the D_2 events due to the plotting procedure.

from the hit pattern caused by the two-fragment channel $HD+D$ as the comparison with Fig. 2(d) shows, is assigned to the $HD+D$ channel.

An example for the extracted position distribution of fragments for a single fragment channel is given in Fig. 7, where the positions of the D_2 (red) and the H (black) fragment of the D_2+H channel following the DR of D_2H^+ at $E_d = 0$ eV are shown in form of a scatter plot. One can clearly see the two circular shapes corresponding to the fragments with mass numbers 1 and 4, respectively.

From the positions x_i and y_j and the mass numbers A_{x_i} and A_{y_j} the (transversal) center-of-mass position (x_{cm}, y_{cm}) is calculated. The resulting x- and y-distributions of the center-of-mass position for events following the DR of D_2H^+ at $E_d = 0$ eV are shown in Fig. 8. The data was taken 30s after injection and continuous electron cooling, and exemplifies the good phase-space cooling that can be reached with the electron target of the TSR; taking the width of the strips into account the center-of-mass spread at the position of the detector is estimated to be $\lesssim 0.9$ mm (FWHM) in x- as well as in y-direction. In the further analysis of the data only events within a 2σ -ellipse around the centroid of the center-of-mass distribution are used to further suppress background events which might result from dissociative charge exchange reactions of the molecular ion with the residual gas of the TSR.

To investigate the influence of the detector properties and of the approximations and cuts used in the data analysis on the deduced results, and to allow for a detailed comparison with theoretical predictions for the DR pro-

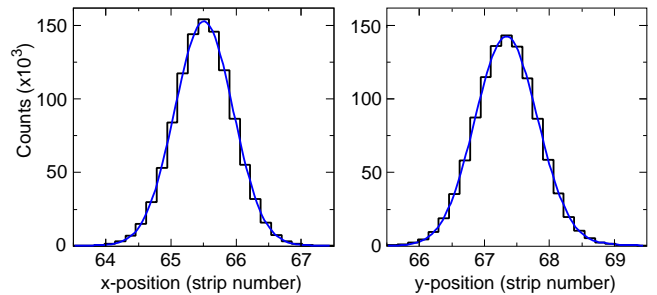


FIG. 8: The horizontal and vertical distribution of the center-of-mass coordinates of DR events of D_2H^+ taken after 30 s of phase-space cooling at collision energies of $E_d = 0$ eV. The blue lines are fits by a Gaussian distribution.

cess, a Monte Carlo simulation program has been developed. The simulation creates DR events at random position in the overlap region between the molecular ion beam and the electron beam and propagates them towards the detector. Subroutines are available to allow for an internal excitation of the ion and to incorporate different kinetic energy releases and angular distributions of the fragments with respect to the center-of-mass direction. At the detector, the impact position for each fragment is determined, which includes the decision as to which part of the entrance window was hit. The kinetic energy loss in the appropriate dead layer is subtracted for each fragment and a pulse proportional to the remaining kinetic energy is created on the strip being hit, broadening the pulse height by a Gaussian shaped resolution function. For fragments hitting the same strip the pulse heights are added. If the gap between two x-strips is hit, the fragment is assumed not to be detected. If the impact position happens to be in the gap between two y-strips of the back side, the signal is shared. The output of the program for a simulated event is a list of strip numbers and corresponding pulse heights. The simulated data are then treated with the same analysis tools as the measured data.

V. RESULTS FOR THE DR OF D_2H^+

A. Branching ratio at $E_d = 0$ eV

The branching ratios for the three final fragment channels accessible in the DR of D_2H^+ at relative ion-electron energies of $E_d = 0$ eV were determined by analyzing data taken after 30-50s of electron cooling. Although the phase space cooling of the ion beam and the vibrational cooling of the ions is achieved already after ~ 3 s of electron cooling, the cooling was continued in order to lower the rotational temperature of the ions to values below the ambient room temperature of 300 K as shown in Ref. [4]. The relative number of DR events leading to the three fragmentation channels (see Eq. (1)) are $N_\alpha=76.69(4)\%$, $N_\beta=14.32(4)\%$, and $N_\gamma=8.99(3)\%$,

TABLE I: Branching ratios obtained in the present experiment for the three fragment channels following the DR of D_2H^+ at $E_d = 0$ eV. The results are compared to those of a recent measurement at CRYRING [5].

Channel	This work	CRYRING[5]
(α) H+D+D	78.0(0.4)	76.5(2.2)
(β) HD+D	13.5(0.3)	13.5(1.5)
(γ) D ₂ +H	8.6(0.2)	10.0(0.7)

where the uncertainties given are of purely statistical origin. The Monte Carlo simulation was used to correct the measured numbers for the slightly different efficiencies for detecting and identifying the fragment channels. In this simulation the angular distributions of the fragments were assumed to be isotropic, but the population of the different vibrational states of the HD and D₂ fragments as determined in Sec. V C was explicitly taken into account. The resulting corrections which had to be applied to the measured relative numbers given above amount to less than two percentage points.

The deduced branching ratios B are compiled in Table I. The uncertainties given are dominated by systematic errors caused mainly by the not yet fully understood detection efficiency for fragments hitting the gap regions. The ratios are compared to the result of a recent measurement performed at CRYRING [5] using the grid method. Within the error bars the two measurements agree well despite the presumably different initial rotational temperatures of the D_2H^+ ions (see also the following section). As discussed already in Ref. [5] the branching ratios display a clear isotope effect: On a purely statistical ground the HD+D channel should be twice as strong as the D₂+H channel, i.e., in the absence of an isotope effect one would expect $2B(D_2+H)/B(HD+D) = 1$. However, the measured values result in a deuteration enhancement of $2B(D_2+H)/B(HD+D) = 1.27(0.05)$, slightly smaller than deduced in Ref. [5] but very similar to the ratio $B(HD+H)/2B(H_2+D) = 1.20(0.05)$ observed in the DR of H_2D^+ [3]. These results clearly show that in the DR of deuterated H_3^+ the formation of the two-body fragment channels containing the most deuterons is enhanced.

B. Branching ratios at $E_d > 0$ eV

To determine the branching ratios into the three fragment channels at relative ion-electron energies $E_d > 0$ eV, data collection was started after 3 seconds of electron cooling when the ion beam was already fully phase space cooled. Moreover, at this time all ions are vibrationally relaxed while the rotational temperature is expected to be around 300 K or even slightly higher [4]. Comparing the branching ratios at $E_d = 0$ eV obtained after the shorter phase space cooling with those discussed in Sec. V A, no difference was noticeable within the limits of precision. After electron cooling, the energy of the

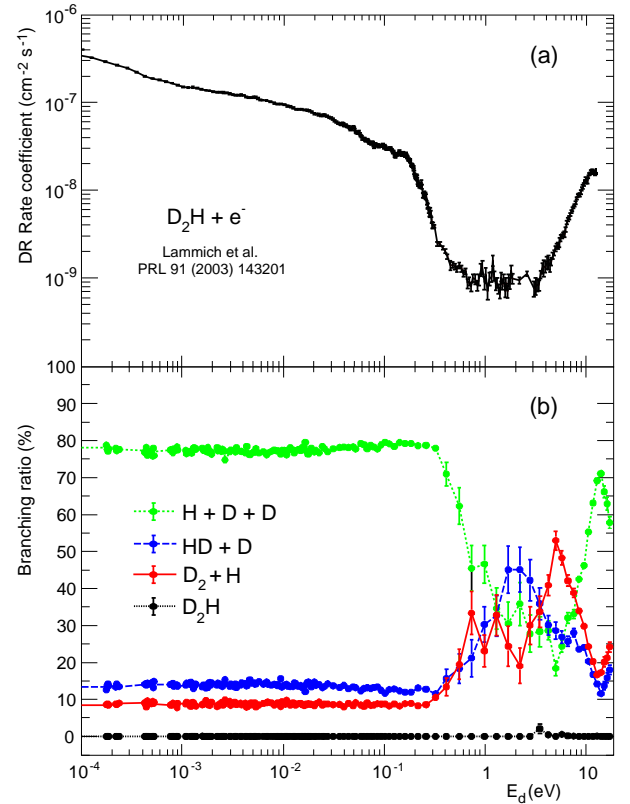


FIG. 9: (a) Energy dependence of the DR rate coefficient of D_2H^+ as measured by Lammich *et al.* [4]. (b) Fragment channel branching ratios determined in the present work as a function of the collision energy with only statistical uncertainties. In the absence of isotope effects one expects to find $B(HD+D) = 2B(D_2+H)$.

electron beam was frequently switched between the cooling energy and the desired detuning energy $E_d > 0$ eV, changing the latter from injection to injection to span the range between 0 up to 20 eV. The detuning-energy cycle was repeated several times to collect statistically reliable data. The branching ratio at each detuning energy was then obtained as described in Sec. V A, including the corrections due to the slightly different detection efficiencies for the three fragment channels. Efficiency losses that could occur at high detuning energies due to the finite size of the detector were shown to be insignificant by investigating the distribution of impact positions of the fragments on the detector; at high detuning energies a considerable part of the maximal available release energy is not converted into kinetic energy of the fragments, but into internal excitation energy of the fragments. Moreover, background events from dissociative charge exchange collisions with the residual gas were found to be negligible at all measured ion-electron energies.

Figure 9 shows the extracted fragment channel branching ratios in the range of $E_d = 0.2$ meV to 20 eV together with the DR rate coefficient measured in a previous ex-

periment at the TSR under similar cooling conditions [4]. As to be expected, the probability for the recombination channel D_2H , which requires the emission of a stabilizing photon in times comparable to the dissociation times, is found to be consistent with zero to within better than 1%. The branching ratios into the fragmentation channels are observed to be more or less constant up to $E_d \approx 300$ meV at values close to those obtained at $E_d = 0$ eV, even though the DR rate coefficient drops by two orders of magnitude. In particular, the isotope effect observed at $E_d = 0$ eV persists over this energy range and is even increasing for energies $\gtrsim 300$ meV. For higher energies the branching into the three-body channel is declining quickly and reaches a minimum level of about 20 % between 4 and 5 eV, while the relative intensities of the two-body channels are both rising. At $E_d = 2$ eV the $HD+D$ channel is the dominant fragmentation channel ($B(HD+D) \sim 45\%$), but at around 5 eV the D_2+H channel is even reaching $B(D_2+H) \sim 55\%$, exhibiting a huge isotope effect of $2B(D_2+H)/B(HD+D) = 3.7(0.5)$. At energies above 10 eV the three-body channel regains its role as the dominant fragment channel with a branching ratio above 60 %.

We are not aware of earlier measurements of the fragment branching ratios following the DR of D_2H^+ at detuning energies $E_d > 0$ eV. However, Datz *et al.* [3, 9] have measured these ratios in the energy range between ~ 1 meV and 20 eV for the DR of H_3^+ and its isotopomer H_2D^+ . The overall behavior of the relative branching ratio between the combined two-body channel and the three-body channel is rather similar for all three systems investigated, and the gross structure of this ratio has been successfully attributed to the successive opening of the electronically excited two-body fragment channel $H(nl)+H_2(X^1\Sigma_g)$, $H(2l)+H_2(B^1\Sigma_u)$ and of the three-body channel $H(2l)+H(1s)+H(1s)$ within a statistical approach [10]. However, while in the DR of H_2D^+ the relative fractions of the two two-body channels seem to stay constant over the measured range of energies, we find that this fraction strongly changes in the DR of D_2H^+ at energies between $\sim 1 - 10$ eV, leading to a drastic isotope effect around $E_d \sim 5$ eV that is yet to be explained.

C. Vibrational excitation of fragment molecules

Standard imaging techniques without mass identification have difficulties identifying and separating two-body fragmentation channels in DR experiments involving polyatomic molecular ions. The event-by-event mass identification of all fragments provided by the EMU system allows for a straight-forward analysis of these channels.

The normalized projected distance distributions $P(d)$ for the two two-body fragment channels D_2+H and $HD+D$ observed in the DR of D_2H^+ at $E_d = 0$ eV are displayed in Fig. 10 using data collected after 30 s of electron cooling. Following common practice (see e.g.,

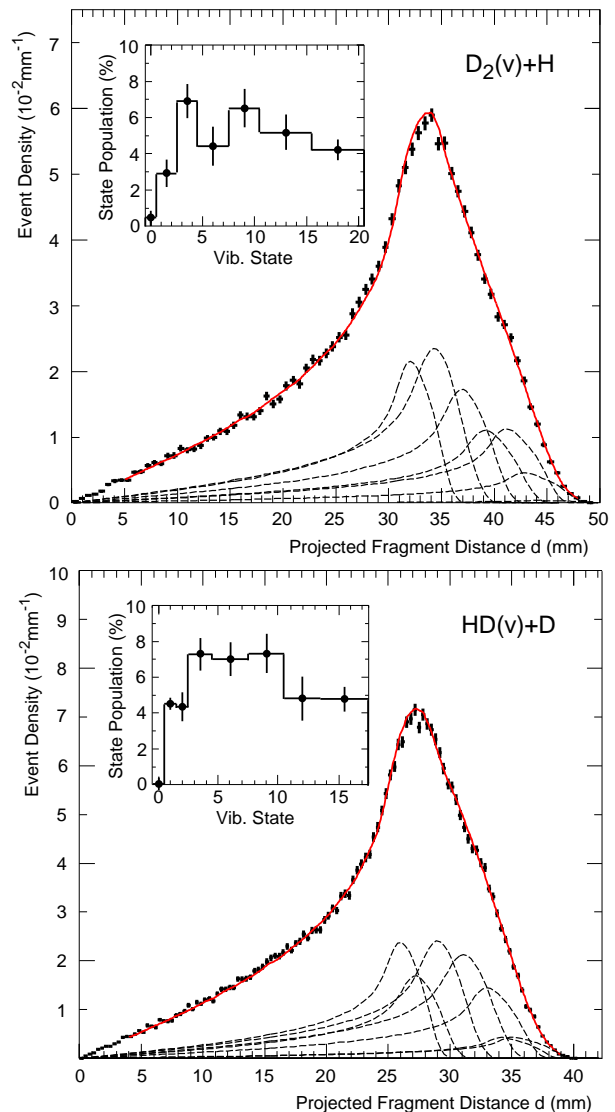


FIG. 10: Normalized projected distance distributions for the two-fragment channels D_2+H (upper panel) and $HD+D$ (lower panel) observed in the DR of D_2H^+ at $E_d = 0$ eV; the solid lines are the result of a fit with simulated distributions (dashed lines) corresponding to the population of different vibrational levels $D_2(v)$ and $HD(v)$, respectively. The resulting population probabilities are shown in the inserts; for histogram bins spanning more than one unit in v , the relative populations were forced to be equal within the bin.

Ref. [11]), the distance $d = ((x_1 - x_2)^2 + (y_1 - y_2)^2)^{1/2}$ between the two fragments in the detector plane is plotted rather than the weighted projected distance D defined by Eq. (6). The projected distance distributions $P(d)$ carry information about the kinetic energy release as well as about the angular distribution of the fragments with respect to the ion (electron) beam direction [12]. Since at $E_d = 0$ eV the angular correlations are expected to be isotropic for symmetry reasons, $P(d)$ can be readily analyzed to yield the kinetic energy release distribution.

In both channels only the vibrational states built

on the electronic ground state of the fragments are energetically accessible, i.e., the available final states are $D_2(X^1\Sigma_g(v))+H(1s)$ with $v=0$ to 20 and $HD(X^1\Sigma_g(v))+D(1s)$ with $v=0$ to 17, respectively. The relative populations of these states, which are derived from a fit of the projected distance distributions $P(d)$ using simulated distributions for individual vibrational states, are shown in the inserts. In the simulation we assume the rotational temperature of the parent ion to be 100 K (see also further below) and the DR rate coefficients to be constant for all rotational angular momenta. For these fits some vibrational levels were grouped together and an equal population was assumed within each group to reduce the uncertainties caused by the anticorrelation of contributions between energetically close levels; they are nevertheless still dominating the accuracy of the deduced populations.

The derived population distributions of the vibrational levels for the molecular fragment are similar for both channels and similar to the distributions measured by Strasser *et al.* [11] in the DR of H_3^+ and D_3^+ . They all show a bell shape-like behavior, close to what is expected from a simple phase space argument [10].

D. The three-body channel H+D+D

Also in studies of DR fragmentation channels which result in a total breakup of the molecule into its atomic constituents, the EMU system has some advantages as compared to standard imaging techniques based on micro-channel plates and an optical readout, even though the latter usually exhibits a considerably better position resolution (e.g., $< 100 \mu m$ [12] as compared to $\sim 750 \mu m$ of the EMU detector). Besides the unambiguous fragment identification, the advantage is in particular the high data rate of up to 2000 Hz that can be handled by the EMU system (to be compared to, e.g., ~ 30 Hz of the TSR optical imaging setup [12]).

In the DR of D_2H^+ at $E_d = 0$ eV the three atomic products can only be formed in their electronic ground states. The total kinetic energy release E_k in the D+D+H channel is thus uniquely determined by the ground state energy release Q_0 of D_2H^+ with respect to the asymptotic free neutral atomic products plus the remaining excitation energy of the D_2H^+ molecule, which we describe by a (rotational) temperature. As discussed in Sec. II, the weighted projected distance D^2 , which is not affected by any of the ambiguities in the fragmentation geometry determination, is proportional to the transverse energy release. The distribution of the weighted projected distances D^2 thus provides information on the total kinetic energy release.

The measured distribution, derived from data collected after 30 s of electron cooling, is plotted in Fig. 11 together with the simulated distribution, which was calculated assuming that the three fragments are isotropically distributed in the available phase space and also assum-

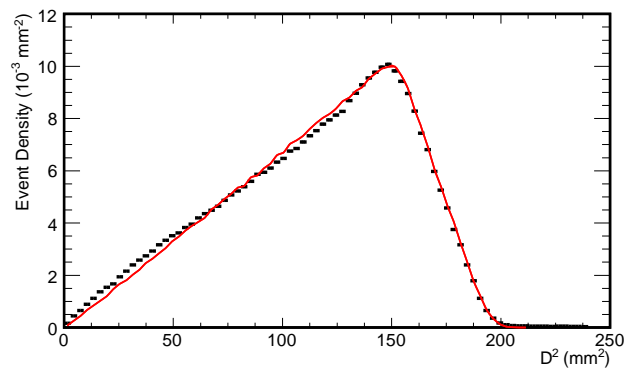


FIG. 11: Normalized distribution of weighted transverse distances D^2 observed in the DR of D_2H^+ at $E_d = 0$ eV for the fragment channel H+D+D after 30 s of phase-space cooling. The solid line is the result of a simulation assuming an isotropic breakup geometry and an initial rotational excitation of the D_2H^+ ions corresponding to a rotational temperature of 100 K.

ing $Q_0 = 4.67$ eV and a rotational temperature of 100 K. While the edge of the distribution at large D^2 , which is most sensitive to the total kinetic energy release, is very well described by the simulation assuming a subthermal rotational temperature of 100 K (see also Ref. [4]), there are small but statistically relevant deviations on the left shoulder of the distribution, which are likely caused by anisotropies in the momentum distribution between the three fragments.

Although we only have access to the transverse kinetic energies of the fragments, it has been shown before [6, 11] that information about the momentum distribution between the three fragments can be gained employing a slightly modified concept of Dalitz coordinates and Dalitz plots. The coordinates η_1 and η_2 originally introduced by Dalitz [13] are linear combinations of the kinetic energies E_i of the three fragments in the center-of-mass frame, taking into account energy and momentum conservation. By plotting the number of events as a function of η_1 and η_2 , the momentum correlations between the fragments can be visualized. In particular, for a purely statistical, phase-space dominated breakup the Dalitz plot is evenly populated. The modified concept [6, 11, 14, 15] consists in defining projected Dalitz coordinates Q_1 and Q_2 by replacing E_i by the corresponding transverse energy $E_{\perp,i}$ and by plotting the number of events as a function of Q_1 and Q_2 instead of η_1 and η_2 . The measured distribution is then divided by a simulated distribution assuming a phase-space dominated breakup in order to account for possible detection efficiency variations and to regain a uniformly populated Dalitz plot in case no momentum correlations between the fragments exist. We will refer to these plots as Dalitz ratio plots.

In the case of the DR of D_2H^+ where two of the three fragments are identical, the projected Dalitz coordinates

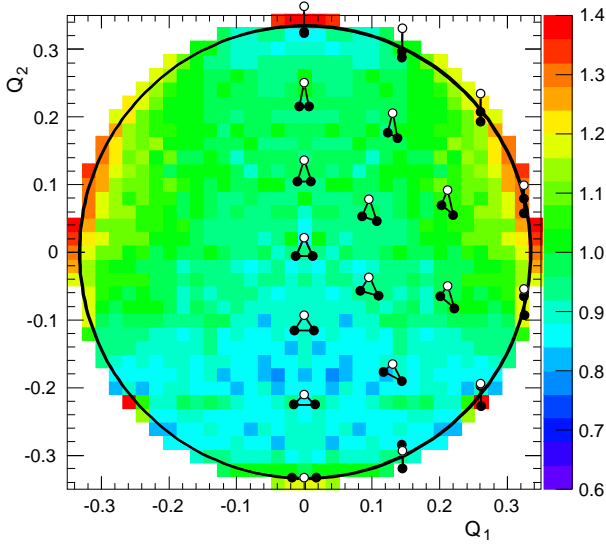


FIG. 12: Dalitz ratio plot of the three-body fragmentation channel following the DR of D_2H^+ at $E_d = 0$ after 30 s of electron cooling. The triangles depict projected dissociation geometries for a sample of points in the (Q_1, Q_2) plane; the white dot shows the position of the H, the black points the positions of the Ds.

Q_1 and Q_2 are conveniently defined as [14]

$$Q_1 = \sqrt{\frac{A}{A_H}} \frac{E_{\perp, D_2} - E_{\perp, D_1}}{3E_{\perp}} \quad (8)$$

$$Q_2 = \frac{A}{3A_D} \frac{E_{\perp, H}}{E_{\perp}} - \frac{1}{3} \quad (9)$$

with

$$E_{\perp, i} = \frac{A_i}{A} [(x_i - x_{cm})^2 + (y_i - y_{cm})^2] \frac{E_B}{S^2} \quad (10)$$

and $E_{\perp} = \sum E_{\perp, i}$. The allowed values of Q_1 and Q_2 are confined by $Q_1^2 + Q_2^2 < 1/9$.

In filling the Dalitz ratio plot two ambiguities have to be considered. The first is connected with the indistinguishability of the two Ds, which leads to two entries: at (Q_1, Q_2) and $(-Q_1, Q_2)$. The second one is specific to the EMU system and is caused by the ambiguity [see Figs. 2(a) and 2(b) and Eq. (10)] in deducing the breakup geometry from the hit pattern. This leads to two additional entries at (Q'_1, Q_2) and $(-Q'_1, Q_2)$ and to a smearing of structures along the Q_1 coordinate. The resulting Dalitz ratio plot, divided by the distribution for an isotropic breakup of D_2H^+ , is shown in Fig. 12. It is quite obvious that the momentum distribution is far from being isotropic and that linear decay geometries are enhanced by up to 40%, where one of the Ds and the H are emitted back-to-back with the second slow D remaining in the center.

The present result agrees with the result obtained in Ref. [6] using standard 2D-imaging, but the almost two order of magnitude higher event rates that can be han-

dled by the EMU system are resulting in improved statistics and thus in a considerably clearer picture. The statistics which can now be attained in these measurements should finally be sufficient to employ the Monte Carlo image restoration technique discussed in Ref. [6] with strongly reduced artificial noise patches. This will allow for a more quantitative analysis of the momentum distributions.

VI. SUMMARY

The potential of the EMU imaging system for studying the dissociative recombination of polyatomic molecular ions with electrons in merged beam experiments is clearly borne out by the results obtained for the DR of D_2H^+ . The main advantage of the new set up, which is based on a large area, energy and position sensitive Si detector with multi-hit capabilities, is the possibility to determine the individual masses of the fragments on an event-by-event basis. This allows one to efficiently distinguish DR events leading to only neutral fragments from DR and background events involving charged fragments, to uniquely identify these fragmentation channels, and to determine their branching ratios as a function of the relative ion-electron energy. While the position resolution, which is limited by the width of the read-out strips to $\sim 750 \mu m$, cannot compete with the resolution of $< 100 \mu m$ of optical imaging systems, it is nevertheless sufficient to allow for detailed studies of total kinetic energy releases and transverse breakup geometries of the different fragmentation channels by 2D imaging; the lack of position resolution is at least partly compensated by the ~ 100 times higher event rate that can be handled by the EMU system, resulting in data of high statistical quality. Moreover, in DR studies of polyatomic molecular ions involving heavier fragments, also the smaller minimum distance between two fragments that can be resolved by the EMU detector as compared to MCP/CCD-based 2D-imaging systems can be an additional advantage.

Comparing the results obtained in the present investigation of the DR of D_2H^+ with results of earlier measurements, where available, generally good agreement is observed. In particular, the branching ratios of 78.0(0.4)%, 13.5(0.3)% and 8.6(0.2)% measured at $E_d = 0$ eV for the $D+D+H$, $HD+D$, and D_2+H channels, respectively, confirm the results recently obtained at CRYRING [5] using the transmission-grid method. The branching ratios as a function of collision energy were measured for the first time. While the general trend of the ratio of the combined two-body to the three-body fragmentation channel looks rather similar to what has been observed before for H_3^+ [9] and H_2D^+ [3], the relative branching ratios between the D_2+H and $HD+D$ channels display an unexpectedly large isotope effect. Whereas the ratio $2B(D_2+H)/B(HD+D)$ is expected to be 1 in the absence of any isotope effect, this ratio is found to be enhanced

by about 25% at most energies investigated, and moreover reaches a so far unexplained large value of 3.7(0.5) at $E_d \sim 5$ eV.

Acknowledgments

HB acknowledges partial support from the German-Israeli Foundation for Scientific Research and Develop-

ment (G.I.F.) under Grant I-900-231.7/2005 and by the European Project ITS LEIF (HRPI-CT-2005-026015). DS acknowledges support by the Weizmann Institute of Science through the Joseph Meyerhoff program. Support by the Max-Planck Society is acknowledged.

-
- [1] M. Larsson and A. E. Orel, *Dissociative Recombination of Molecular Ions* (Cambridge University Press, Cambridge, 2008).
 - [2] F. Sprenger, M. Lestinsky, D. A. Orlov, D. Schwalm, and A. Wolf, Nucl. Instrum. Methods A **532** 298 (2004); D. A. Orlov, U. Weigel, D. Schwalm, A. S. Terekhov, and A. Wolf, *ibid.* **532** 418 (2004); M. Lestinsky *et al.*, Phys. Rev. Lett. **100** 033001 (2008).
 - [3] S. Datz, M. Larsson, C. Stromholm, G. Sundström, V. Zengin, H. Danared, A. Källberg, and M. af Ugglas, Phys. Rev. A **52** 2901 (1995).
 - [4] L. Lammich *et al.*, Phys. Rev. Lett. **91** 143201 (2003).
 - [5] V. Zhaunerchyk, R. D. Thomas, W. D. Geppert, M. Hamberg, M. Kaminska, E. Vigren, and M. Larsson, Phys. Rev. A **77** 034701 (2008).
 - [6] D. Strasser, L. Lammich, H. Kreckel, M. Lange, S. Krohn, D. Schwalm, A. Wolf, and D. Zajfman, Phys. Rev. A **69** 064702 (2004).
 - [7] www.micronsemiconductor.co.uk
 - [8] www.mesytec.de
 - [9] S. Datz, G. Sundström, Ch. Biedermann, L. Broström, H. Danared, S. Mannervik, J. R. Mowat, and M. Larsson, Phys. Rev. Lett. **74** 896 (1995).
 - [10] D. Strasser, J. Levin, H. B. Pedersen, O. Heber, A. Wolf, D. Schwalm, and D. Zajfman, Phys. Rev. A **65** 010702(R) (2001).
 - [11] D. Strasser, L. Lammich, H. Kreckel, S. Krohn, M. Lange, A. Naaman, D. Schwalm, A. Wolf, and D. Zajfman, Phys. Rev. A **66** 032719 (2002).
 - [12] S. Novotny *et al.* Phys. Rev. Lett. **100** 193201 (2008).
 - [13] R. H. Dalitz, Philos. Mag. **44** 1068 (1953)
 - [14] L. Lammich, PhD-thesis (Univ. Heidelberg, 2004), www.ub.uni-heidelberg.de/archiv/4833
 - [15] I. Nevo *et al.*, Phys. Rev. A **76** 022713 (2007).